國 立 交 通 大 學

電信工程學系

碩 士 論 文

環形耦合器之廣義合成及
其電路微小化之應用

Generalized Synthesis of a Rat Race Ring Coupler and Its Application to Circuit Miniaturization

研 究 生：蔡正修 (Cheng-Hsiu Tsai)

指導教授：郭仁財 博士 (Dr. Jen-Tsai Kuo)

中 華 民 國 九十八 年 七 月

環形耦合器之廣義合成及其電路微小化之應用

Generalized Synthesis of a Rat Race Ring Coupler and

Its Application to Circuit Miniaturization

研 究 生：蔡正修　　　　Student：Cheng-Hsiu Tsai

指導教授：郭仁財　博士　　Advisor：Dr. Jen-Tsai Kuo

國 立 交 通 大 學

電 信 工 程 學 系

碩 士 論 文

A Thesis

Submitted to Department of Communication Engineering

College of Electrical and Computer Engineering

National Chiao Tung University

in partial Fulfillment of the Requirements

for the Degree of

Master of Science

in

Communication Engineering

July 2009

Hsinchu, Taiwan, Republic of China

中 華 民 國 九十八 年 七 月

環形耦合器之廣義合成及
其電路微小化之應用

研究生： 蔡正修　　　　　　指導教授： 郭仁財 博士

國立交通大學 電信工程學系

摘要

　　本論文的第一部分闡述環形耦合器的廣義合成，根據環形耦合器必須滿足的條件，使用傳輸線理論及奇偶模分析可推論得到所有的電路參數，由數學分析可得知：我們可以設計出無限多組電路。為了驗證本論文提出的理論，我們設計一個周長為 0.97 個波長(傳統環形耦合器周長為 1.5 個波長)的電路，它的面積只占傳統環形耦合器的 41.82%. 某些廣義環形耦合器的頻寬模擬值也被提出並探討，頻寬與電路尺寸之間的關係也在此做深入的討論。

　　第二部分研究步階式阻抗對於電路微小化的影響。將環形耦合器的四段傳輸線等效代換成步階式阻抗，不但仍保持環形耦合器的特性，而且可縮短電路的周長。論文第一部份設計出的電路若使用此方法可以有效地縮小電路，如果此電路的中心頻率設計在 1 GHz, 縮小後的電路面積只會占傳統耦合器的 13.12%, 我們相信，在目前的開放文獻中，這個電路的面積是所有微帶線環形耦合器中最小的一個。

　　論文中包含兩組實作電路，它們的量測結果證實與模擬值吻合。

Generalized Synthesis of a Rat Race Ring Coupler and Its Application to Circuit Miniaturization

Student: Cheng-Hsiu Tsai   Advisor: Dr. Jen-Tsai Kuo

Department of Communication Engineering

National Chiao Tung University

Abstract

Generalized synthesis of the rat race ring coupler is developed with its four arms being allowed to have different characteristic impedances and electrical lengths. The transmission line theory incorporated with the even-odd analysis is used to formulate the conditions for solving the circuit parameters. The solution shows that a rat race ring with a normalized area of 41.82% or 0.97λ-circumference can be achieved. Based on the solutions, simulated bandwidths of the new ring hybrids are reported. Two experimental circuits are measured for validation check. One uses stepped-impedance sections to realize the four arms for further size reduction. This circuit occupies only 13.12% of that of a conventional hybrid ring at 1 GHz. It is believed that this implementation has the best size reduction for a microstrip ring hybrid in open literature. Measured scattering parameters show good agreement with the simulated results.

誌　謝

　　轉眼間，我即將從碩士班畢業，在這兩年裡我學到很多，這都歸功於交大提供我良好的研究環境，以及周遭很多人的幫助。

　　首先我想感謝我的指導教授：郭仁財老師。他對研究無比的熱情影響我很深遠，他對我的鞭策也讓我做研究更有效率。接著我要感謝學長姐的指導，不管是研究上的問題，或是實作電路的經驗傳承，他們的指點讓我事半功倍。其中我特別要感謝逸群學長，在研究遇到瓶頸的時候，他的建議總會給我對的方向。我同時也要感謝實驗室的同學和學弟妹，和他們一起討論也使我從中有所獲得。

　　最後我要謝謝我的家人和朋友，感謝他們的鼓勵與包容，讓我能積極面對眼前的挑戰。有他們的支持，我才能專心地完成研究。

CONTENTS

List of Tables

List of Figures

CHAPTER 1

Introduction

A rat race coupler is one of the fundamental and important passive circuits in RF/microwave front end. It can be incorporated with balanced mixers and balanced amplifiers for equal power division with in- and anti-phase outputs. When the operation frequency is low, the circuit area can be unacceptably large since it has a circumference of $3\lambda/2$ long, where λ is wavelength at the operation frequency. To reduce the circuit size, many approaches have been proposed. In this Chapter, these papers will be reviewed.

1.1   LITERATURE REVIEW
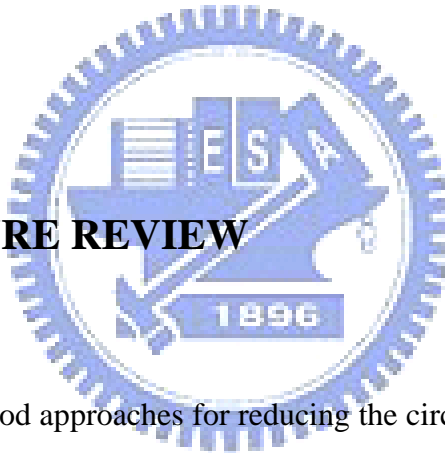
There are lots of good approaches for reducing the circuit size of rat race coupler. The most intuitive way could be to fold the line traces. The folded structure in [1] has four- to five-fold reduction in footprint as compared with the conventional ring hybrid. Incorporation of lumped elements into the coupler is also quite effective for size reduction. For example, the designs in [2] [3] save 70% ~ 80% of the circuit area. The inductors, however, typically have a low quality factor and will degrade the circuit performance.

Many other effective approaches have been reported for miniaturizing distributed rat race couplers. The designs based on the photonic bandgap cells [4] and the compensated spiral compact microstrip resonant cells [5] consume only 60% and 45%,

respectively, of the area of the conventional ring. In [5] ~ [8], phase inverters of $\lambda/4$ long are used to replace the $3\lambda/4$ section of the conventional rat race hybrid, so that the normalized area can be reduced to $(2/3)^2 \approx 44.4\%$. Embedding the patterned apertures in the ground plane under the peripheral of the hybrid can save 64% of the circuit area [9]. The slow wave effect produced by attaching periodical capacitive loads to transmission line sections can also be used to reduce the total length of the ring [10] [11]. The best circuit reduction in [11] achieves a normalized area of 32%.
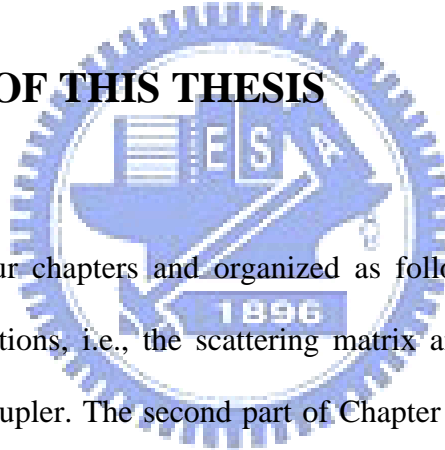
In [12], $\lambda/8$- and $\lambda/6$-sections are proposed to design 3-dB hybrid-ring couplers with $5\lambda/4$ and $7\lambda/6$ circumferences, respectively. The area of the $7\lambda/6$-ring uses about 60% of that of the conventional 1.5λ-ring. In [13], the four sections of the $7\lambda/6$-ring [12] are miniaturized by the stepped-impedance configurations. The circuit shows an area of about 21% of a conventional circuit and no passband up to the sixth harmonic. In addition to size reduction, the stepped-impedance configuration is suitable for designing dual-band devices, e.g., the couplers with equal or arbitrary power divisions in [14] [15], where the 2.45/5.2 GHz rat race couplers use only a normalized area of about 21% at the first band.

In [16], a rat-race coupler with a peripheral of close to 1λ is achieved, and a $19\lambda/18$-ring is realized and measured at 0.9 GHz. In their formulation, the four sections have identical characteristic impedance and three of them are commensurate. In [17], design formulas for a generalized 180° hybrid coupler are presented.

1.2 CONTRIBUTIONS

This thesis extends the derivation in [16] and [17] to a more generalized and detailed fashion. The extension includes that the four arms may have different characteristic impedances and that the three shorter arms may have different lengths. Design equations are derived for calculating the circuit parameters based on the transmission line theory. The solutions show that the circuit circumference can be further reduced to less than 1λ. Based on the solution, size reduction factors and simulation bandwidths for reduced-length couplers are investigated and discussed. In addition, the approach in [13] is employed to replace the four arms at 1 GHz, and it results in a normalized circuit area of 13.12% or 0.54λ-circumference.

1.3   OUTLINE OF THIS THESIS

This thesis has four chapters and organized as follows. Chapter 2 introduces characteristics and functions, i.e., the scattering matrix and circuit parameters of a conventional rat race coupler. The second part of Chapter 2 derives the formulae for synthesizing the ring hybrids. Some solutions are presented and the corresponding circuit bandwidths are discussed. In addition, measured results of an experimental circuit are compared with simulation data for validation of the theory.

In Chapter 3, an application to circuit miniaturization is presented. To reduce the circuit size, stepped-impedance sections are utilized to replace the four arms of a rat race coupler. The technique is based on the transmission line theory and the derivation is given in details. Furthermore, comparison between the rat races with and without stepped-impedance substitutions is also discussed. The measurement results of an experimental circuit are used to validate the simulation results based on the proposed

theory.

Chapter 4 draws the conclusion of this thesis and proposes some suggestions of the future works.
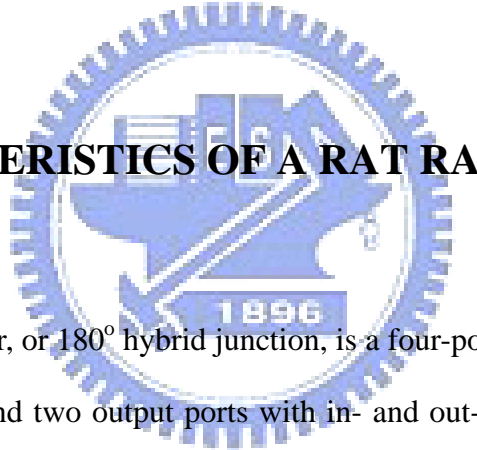
CHAPTER 2

Synthesis of a Generalized Rat Race Coupler

This chapter will first describe basic characteristics of a rat race coupler. Then, derivation for generalized synthesis of a rat race is presented. The design graphs of circuit parameters, including the characteristic impedances and electric lengths, are displayed. Finally, tradeoffs between circuit size and bandwidth are discussed. With the graphs and tables shown in this chapter, a rat race coupler can be readily designed and synthesized.

2.1   CHARACTERISTICS OF A RAT RACE COUPLER

The rat race coupler, or 180° hybrid junction, is a four-port network with an input port, an isolated port, and two output ports with in- and out-of-phase signals. Figure 2.1 shows the circuit schematic of a conventional rat race ring coupler, consisting of an internal ring with impedance $\sqrt{2}\ Z_0$ and four feed lines with identical port impedance Z_0. A signal applied to port 1 will be evenly split into two in-phase components at ports 2 and 4 while port 3 is isolated. If the input is taken at port 2, it will be equally split into two components at ports 1 and 3 with 180° phase difference, and port 4 is isolated. A rat race ring coupler can also be used as a power combiner. When input signal is applied to ports 2 and 4, a half of the sum of the inputs will be formed at port 1, while a half of the difference will be formed at port 3. Therefore, ports 1 and 3 are referred as the sum and difference ports respectively. Thus, the scattering matrix for an ideal 3dB rat race ring coupler has the following form [19]:

$$[S] = \frac{-j}{\sqrt{2}} \begin{bmatrix} 0 & 1 & 0 & 1 \\ 1 & 0 & -1 & 0 \\ 0 & -1 & 0 & 1 \\ 1 & 0 & 1 & 0 \end{bmatrix} \tag{2.1}$$
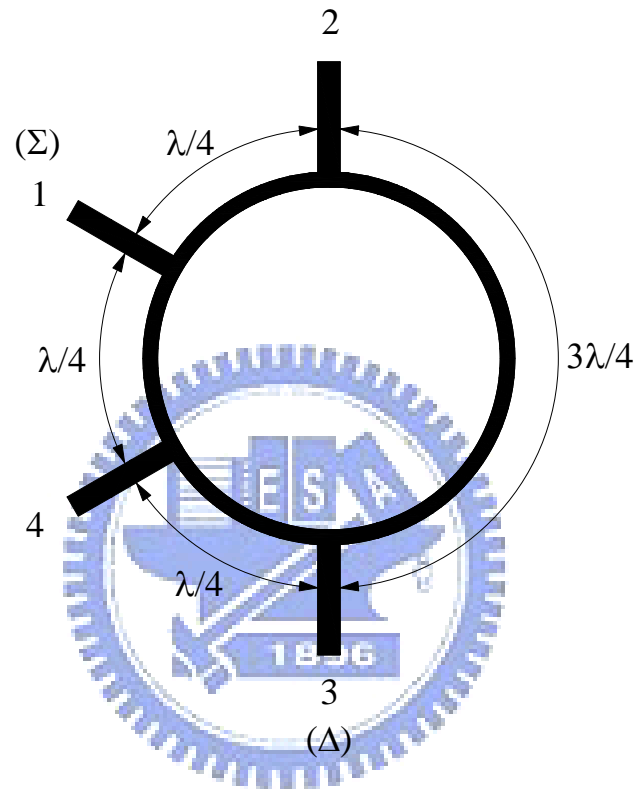

Figure 2.1 Circuit schematic of the conventional rat race coupler.

2.2 GENERALIZED SYNTHESIS

A generalized rat race ring coupler is derived in this section. Both the characteristic impedances and electric lengths of the four arms can be designed by utilizing the provided formulae. In addition, tradeoffs between circuit size and bandwidth are demonstrated and discussed.

2.2.1 Formulation

Figure 2.2 shows the layout of the rat race under investigation of port designation. The reference port admittance is normalized to unity. The parameters Y_i and θ_i ($i = 1$, 2, and 3) represent the characteristic admittances and electric lengths of the sections, respectively. Even- and odd-mode analysis can be used due to the circuit symmetry. Based on even-odd analysis, the four-port network can be reduced to a two-port shown in Figure 2.3. Let jY_a and jY_b be the input admittances seen at ports 1 and 2 looking into the sections loaded with Y_L. The ABCD matrix in Figure 2.3 can be readily derived as

$$A = \cos\theta_2 - \frac{Y_b}{Y_2}\sin\theta_2 \tag{2.2a}$$

$$B = \frac{j\sin\theta_2}{Y_2} \tag{2.2b}$$

$$C = j\cos\theta_2\left(Y_a + Y_b\right) + j\sin\theta_2\left(Y_2 - \frac{Y_a Y_b}{Y_2}\right) \tag{2.2c}$$

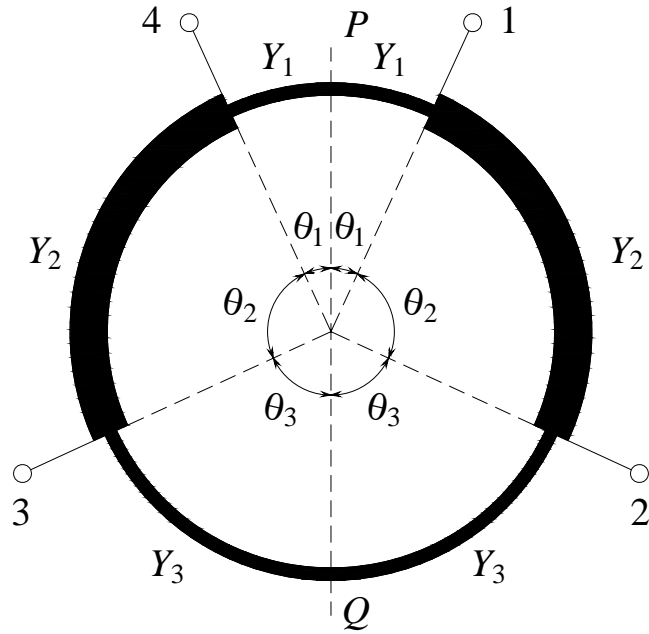$$D = \cos\theta_2 - \frac{Y_a}{Y_2}\sin\theta_2 \tag{2.2d}$$

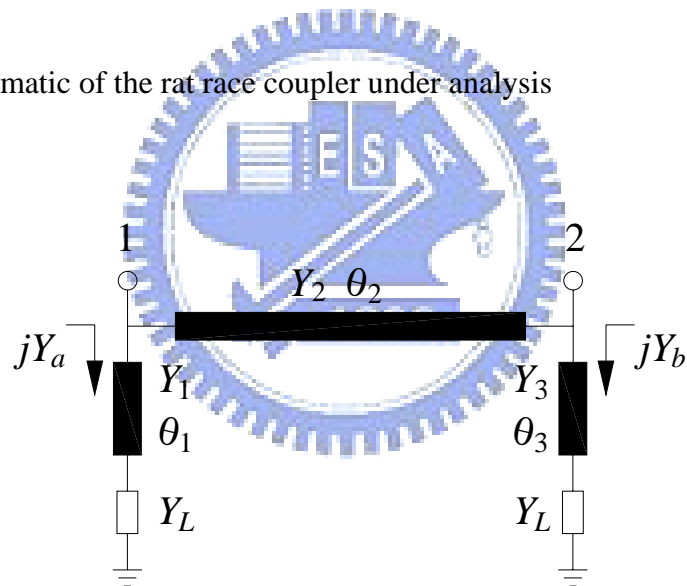Figure 2.2 Schematic of the rat race coupler under analysis

Figure 2.3 Reduced circuit for even- and odd-mode analysis

When $Y_L = 0$, namely, the even-mode, $Y_a = Y_1 \tan \theta_1$ and $Y_b = Y_3 \tan \theta_3$. If the excitation is taken at port 1, the reflection and transmission coefficients can be derived as

$$\Gamma_e = \frac{A + B - C - D}{A + B + C + D} \equiv \frac{E_3 + jE_4}{E_1 + jE_2} \tag{2.3a}$$

$$T_e = \frac{2}{A + B + C + D} \equiv \frac{2}{E_1 + jE_2} \tag{2.3b}$$

where

$$E_1 = \cos\theta_2 \left(2 - \tan\theta_2 \left(\frac{Y_1}{Y_2} \tan\theta_1 + \frac{Y_3}{Y_2} \tan\theta_3 \right) \right) \tag{2.4a}$$

$$E_2 = \cos\theta_2 \left(\frac{\tan\theta_2}{Y_2} + \Delta_e \right) \tag{2.4b}$$

$$E_3 = \sin\theta_2 \left(\frac{Y_1}{Y_2} \tan\theta_1 - \frac{Y_3}{Y_2} \tan\theta_3 \right) \tag{2.4c}$$

$$E_4 = \cos\theta_2 \left(\frac{\tan\theta_2}{Y_2} - \Delta_e \right) \tag{2.4d}$$

$$\Delta_e = Y_1 \tan\theta_1 + Y_3 \tan\theta_3 + \tan\theta_2 \left(Y_2 - \frac{Y_1 Y_3}{Y_2} \tan\theta_1 \tan\theta_3 \right) \tag{2.4e}$$

For the odd mode, $Y_L = \infty$. Then, $Y_a = -Y_1 \cot\theta_1$ and $Y_b = -Y_3 \cot\theta_3$ can be readily obtained. Therefore, the two coefficients can be derived in a similar fashion. Let

$$\Gamma_o = \frac{H_3 + jH_4}{H_1 + jH_2} \tag{2.5a}$$

$$T_o = \frac{2}{H_1 + jH_2} \tag{2.5b}$$

where

$$H_1 = \cos\theta_2 \left(2 + \tan\theta_2 \left(\frac{Y_1}{Y_2}\cot\theta_1 + \frac{Y_3}{Y_2}\cot\theta_3 \right) \right) \tag{2.6a}$$

$$H_2 = \cos\theta_2 \left(\frac{\tan\theta_2}{Y_2} + \Delta_o \right) \tag{2.6b}$$

$$H_3 = \sin\theta_2 \left(\frac{Y_3}{Y_2}\cot\theta_3 - \frac{Y_1}{Y_2}\cot\theta_1 \right) \tag{2.6c}$$

$$H_4 = \cos\theta_2 \left(\frac{\tan\theta_2}{Y_2} - \Delta_o \right) \tag{2.6d}$$

$$\Delta_o = -Y_1\cot\theta_1 - Y_3\cot\theta_3 + \tan\theta_2 \left(Y_2 - \frac{Y_1 Y_3}{Y_2}\cot\theta_1\cot\theta_3 \right) \tag{2.6e}$$

It can be observed that H_k is E_k (k = 1, 2, 3 and 4) by replacing $\tan\theta_1$ and $\tan\theta_3$ with $-\cot\theta_1$ and $-\cot\theta_3$, respectively. Since the coupler is reciprocal and symmetric about the PQ plane, only six entries of its 4×4 S-parameter matrix, i.e., S_{m1} (m = 1, 2, 3 and 4), S_{22} and S_{32} have to be derived. When excitation is taken at port 2, it can be validated that the reflection and transmission coefficients are the results in (2.3) and (2.5) by interchanging the indices 1 and 3.

Next, the following inter-port properties are used to formulate the conditions for solving the circuit parameters:

1) Isolation: $S_{31} = (T_e - T_o)/2 = 0 \Rightarrow E_1 = H_1$ and $E_2 = H_2$. It leads to $Y_1(\tan\theta_1 + \cot\theta_1)$ + $Y_3(\tan\theta_3 + \cot\theta_3) = 0$ and $\tan^2\theta_1 \tan^2\theta_3 = 1$, so that

$$Y_1 = Y_3 \tag{2.6a}$$

$$\theta_3 = \theta_1 \pm \frac{n\pi}{2}, n = 1,3,5,... \tag{2.6b}$$

When excitation is applied to port 2, the same result in (2.6) can be obtained while deriving $S_{42} = 0$.

2) Input matching: $S_{11} = (\Gamma_e + \Gamma_o)/2 = 0 \Rightarrow E_3 = -H_3$ and $E_4 = -H_4$. The same conditions are obtained when $S_{22} = 0$ is used.

3) Outputs: $S_{21} = (T_e + T_o)/2 = \alpha \, S_{41} = \alpha \, (\Gamma_e - \Gamma_o)/2$. It results in $|\alpha| e^{j\phi_1} (E_3 + jE_4)$, where $|\alpha|$ denotes the magnitude of S_{21}/S_{41} while ϕ_1 is the phase difference between the outputs, ports 2 and 4. Thus, two possible results, (2.7) and (2.8), can be obtained.
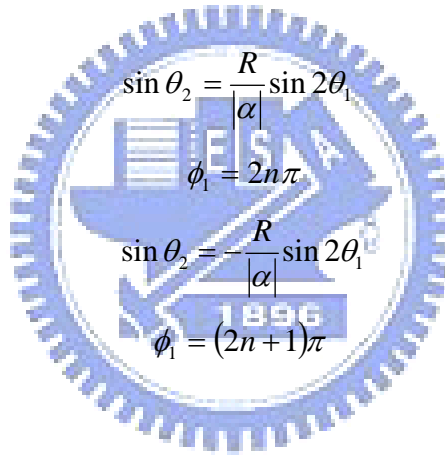
$$\sin\theta_2 = \frac{R}{|\alpha|}\sin 2\theta_1 \tag{2.7a}$$

$$\phi_1 = 2n\pi \tag{2.7b}$$

$$\sin\theta_2 = -\frac{R}{|\alpha|}\sin 2\theta_1 \tag{2.8a}$$

$$\phi_1 = (2n+1)\pi \tag{2.8b}$$

However, θ_1 or θ_2 in (2.8a) must be larger than 90° to satisfy the equation. To minimize the circumference of the coupler, (2.7a) and (2.7b) are used instead of (2.8a) and (2.8b) herein. Similarly, (2.7a) and (2.9) can be obtained when deriving S_{12}/S_{32}. ϕ_2 is the phase difference between ports 1 and 3 while excitation is taken at port 2, and the magnitude of S_{12}/S_{32} is the same as S_{21}/S_{41}, i.e. $|\alpha|$.

$$\phi_2 = (2n+1)\pi \tag{2.9}$$

Based on the results of properties 2) and 3), we have $E_4 = X_4 = 0$. With the aid of (2.6), the following conditions can then be obtained:

$$\frac{1}{Y_1} = \sqrt{1 + R^2 - 2R \cot 2\theta_1 \cot \theta_2} \tag{2.10}$$

where $R = Y_2/Y_1$. In (2.6b), the solution of the minus sign is just that of the plus sign with interchange of θ_1 and θ_3 (See also Figure. 2.2). Therefore, choosing the plus sign will not lose any solution since $Y_1 = Y_3$, as shown in (2.6a). Furthermore, for minimizing the ring size, $n = 1$ is used herein. Based on (2.7a), (2.7b), and (2.9), $|\alpha|$ can be controlled by θ_1, θ_2, and R while the phase difference between two output ports is either 0° or 180°. As shown in Figure 2.4, if R is fixed and $|\alpha|$'s range is designed to be from -10 dB to 10 dB, every θ_1 value results in one specific θ_2 curve. The dashed lines in Figure 2.4 represent the maxima of θ_1, consisting of real solutions of θ_2 for $|\alpha|$ from -10 dB to 10 dB. Namely, $|\alpha|$'s range can not be realized from -10 dB to 10 dB if θ_1 value is larger than the dashed line. Therefore, R and θ_1 must be chosen properly to meet the requirement of $|\alpha|$. Note also that the point A in Figure 2.4(b) denotes the conventional rat race coupler with $\theta_1 = 45^o$, $\theta_2 = 90^o$, and $|\alpha| = 0$ dB.

(a)

(b)

(c)
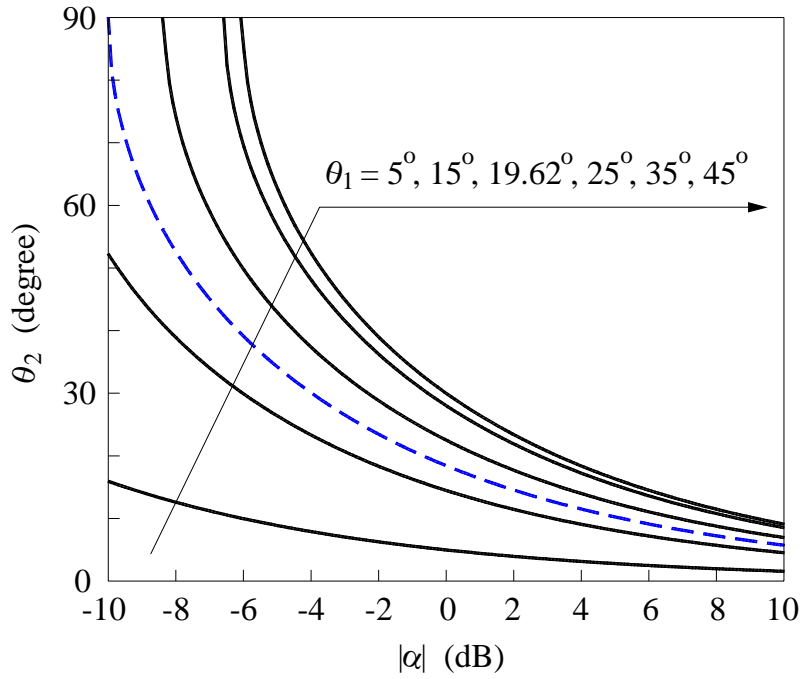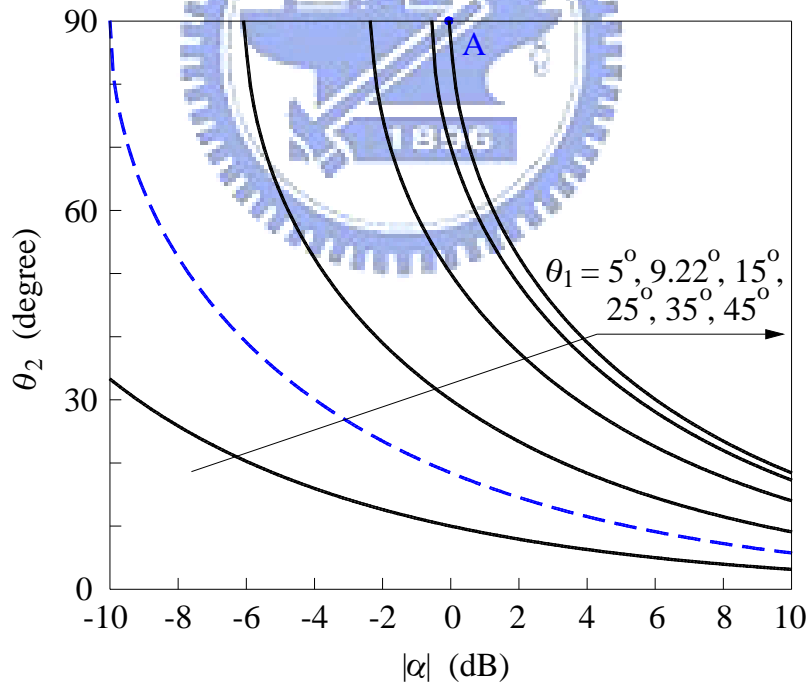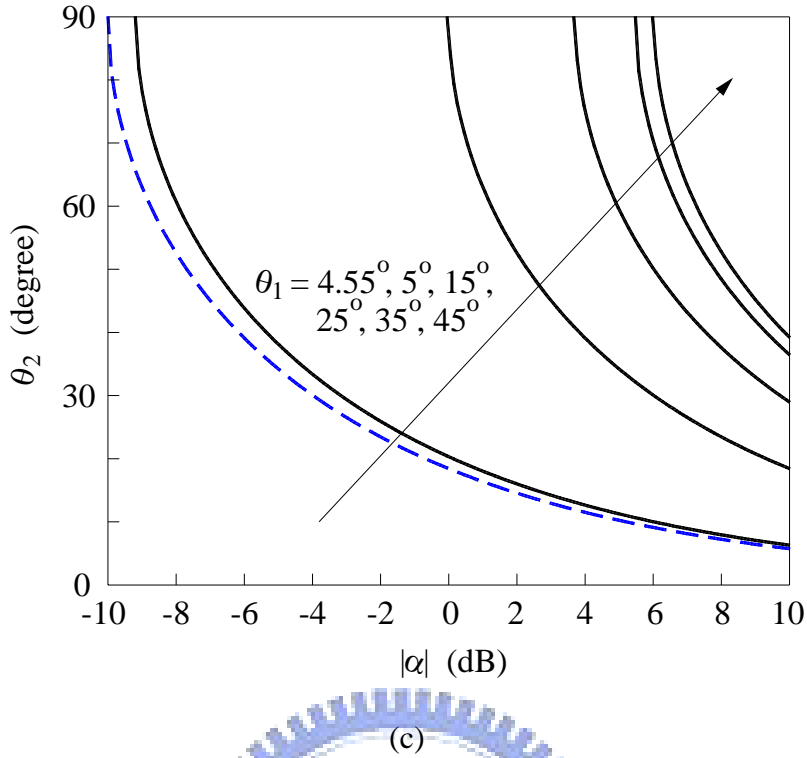
Figure 2.4 θ_2 solutions as functions of $|\alpha|$ for various θ_1 values while R is fixed. (a) R = 0.5. (b) R = 1. (c) R = 2.

For a 3-dB rat race coupler, $|\alpha|$ equals 1. Since 3-dB rat race couplers have been widely used in many applications, we focus on the rat race couplers with $|\alpha| = 1$ below. When $|\alpha|$ is 0 dB, (2.7a) can be written as (2.11). Figure 2.5(a) plots the solution θ_2 versus θ_1 for various R values based on (2.11). One can see that for any θ_1 there are two θ_2 solutions, and vice versa. Note that the solution curves in Figure 2.5(a) are bisymmetric about $\theta_1 = 45^o$ and $\theta_2 = 90^o$. For circuit size miniaturization, only the results in the region of $\theta_1 \leq 45^o$ and $\theta_2 \leq 90^o$ will be considered herein. Similarly, when $R = 1$ we choose $\theta_2 = 2\theta_1$ instead of $\theta_2 = \pi - 2\theta_1$ as the solution to (2.11).

$$\sin \theta_2 = R \sin 2\theta_1 \qquad (2.11)$$

When $R = 1$, it can be readily derived from (2.10) that

$$\frac{1}{Y_1} = \sqrt{2\left(1 - \cot^2 2\theta_1\right)} \qquad (2.12)$$

which is identical to that given in [16], where all the solutions to the ring hybrid design are in one curve of Figure 2.5(b). One can validate that (2.11) and (2.10) are equivalent to (1a) and (1b) of [17]. The condition that θ_1 and θ_2 have to obey in (2) of [17] is an inequality. Here, it has an explicit form in (2.11) and is plotted in Figure 2.5(a). Based on (2.10), Figure 2.5(b) plots the $Z_1 = Y_1^{-1}$ solutions against θ_1. For each R value, the real Z_1 solution exists only within a certain θ_1 range. By enforcing $Z_1 = 0$ in (2.10), it can be derived that the lower θ_1 bound can be calculated by (2.13) and (2.14):

$$\sin 2\theta_1 = \frac{\sqrt{2}}{\left|1 - R^2\right|} \sqrt{\sqrt{2\left(1 + R^4\right)} - \left(1 + R^2\right)} \qquad (2.13)$$

$$\theta_1 \geq \frac{1}{2} \sin^{-1} \left(\frac{\sqrt{2}}{\left|1 - R^2\right|} \sqrt{\sqrt{2\left(1 + R^4\right)} - \left(1 + R^2\right)} \right) \qquad (2.14)$$

For example, when $R = 5$ and 0.2, the lower bounds are $\theta_1 = 5.20^\circ$ and 32.25°, respectively. For the particular case of $R = 1$, $\theta_1 = 22.5^\circ$ can be easily obtained by enforcing $\cot 2\theta_1 = 1$ in (2.10) or by evaluating (2.14) using the L'Hospital's rule. When Z_1 is a small number, say 0.2, the θ_1 value will be close to that given in (2.13) since each curve has a large slope when $Z_1 = 0$. The Z_1 solution curves for $R \geq 1$ have various upper bounds which are also functions of R and can be derived from (2.11):

$$\theta_1 = \sin^{-1}(R^{-1}\sin\theta_2)/2 \leq \sin^{-1}(R^{-1})/2 \tag{2.14}$$

For example, when $R = 5$ and 1.25, the upper bounds are $\theta_1 = 5.77^{\circ}$ and 26.57°, respectively. When $R \leq 1$, the upper θ_1 bounds can be calculated from the corresponding lower bound in (2.14) since the Y_1^{-1} curves are symmetric about $\theta_1 = 45^{\circ}$.

Based on (2.6b) and (2.11), the total circumference of the ring can be expressed in terms of θ_1 as

$$\Phi(\theta_1) = 4\theta_1 + 2\sin^{-1}(R\sin2\theta_1) + 180^{\circ} \tag{2.15}$$

Figure 2.5(c) plots the total length ℓ of the hybrid ring normalized with respect to 1.5λ, or
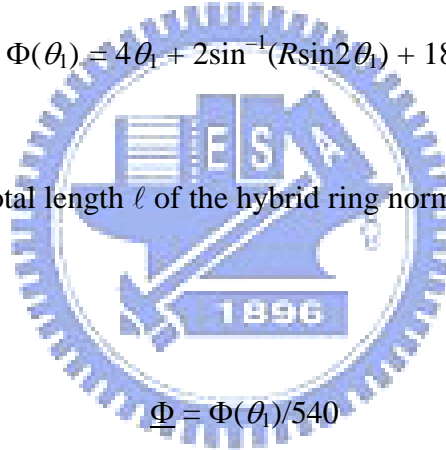
$$\underline{\Phi} = \Phi(\theta_1)/540 \tag{2.16}$$

for the given R values. Note that as compared with the traditional 1.5λ-ring, the normalized area is square of $\underline{\Phi}$.

One can design the circuit starting from a given size reduction, e.g., $\underline{\Phi} = 0.7$, and Figure 2.5(c) shows that there are many possible R values. Alternatively, the design can start from a given θ_1, say $\theta_1 = 30^{\circ} > 22.5^{\circ}$, a smaller R value will lead to a better area reduction. Note that when $R = 1$, as in [16], the best theoretical size reduction is $\ell = \lambda$ (normalized area = 4/9) under the limit of $Y_1^{-1} = 0$ where $\theta_1 = 22.5^{\circ}$. If Y_2 is different from Y_1, i.e., $R \neq 1$, a hybrid ring with $\ell < \lambda$ can be obtained. It is also

possible to start the design from a given Y_1^{-1} in Figure 2.5(b). Once the θ_1 and R values are chosen, θ_2 can be determined by invoking the solution curves in Figure 2.5(a).
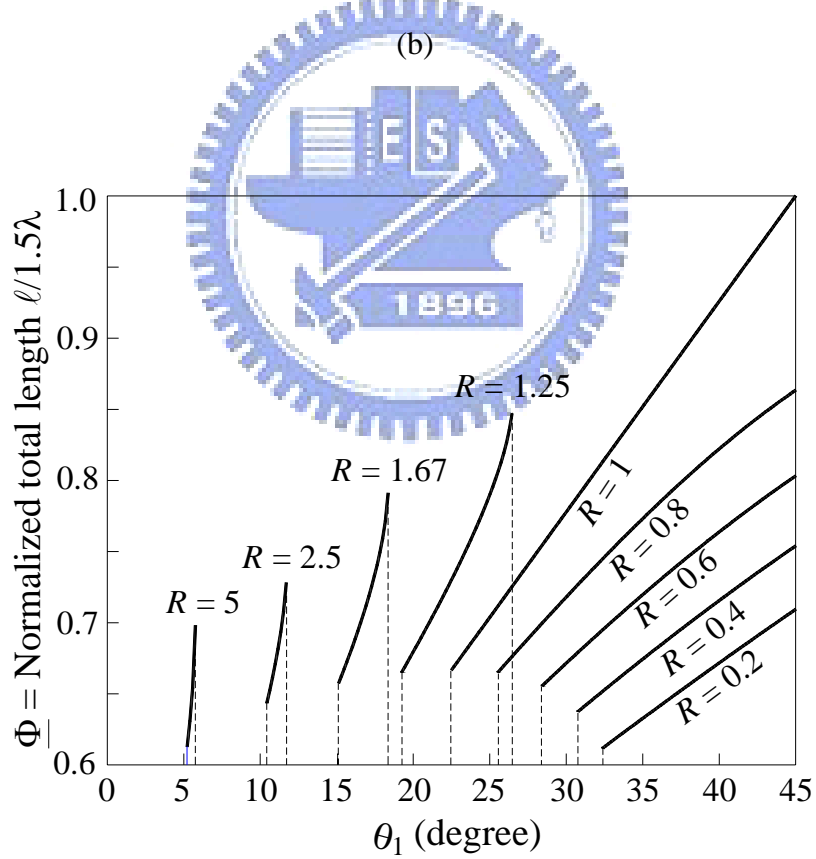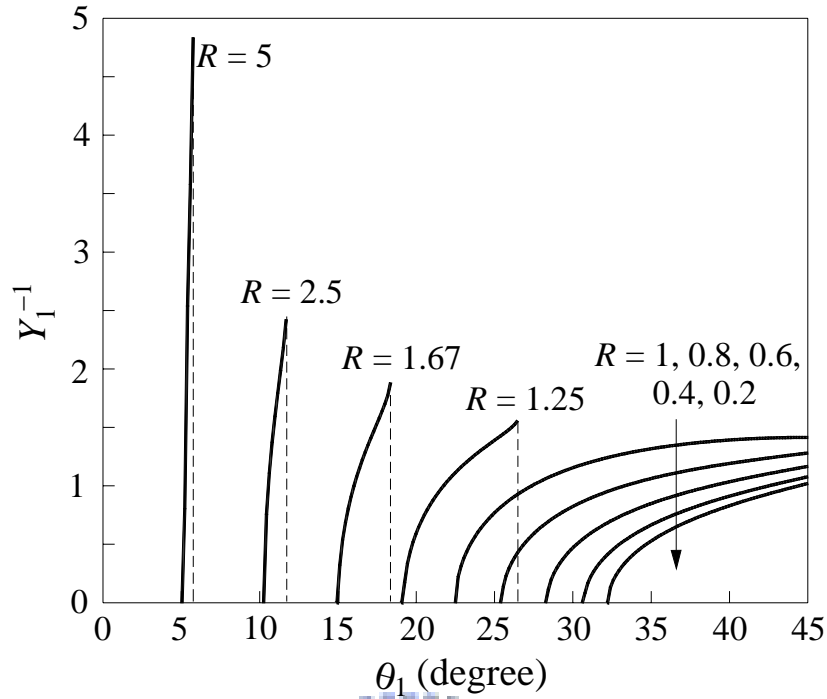

(a)

(b)

(c)
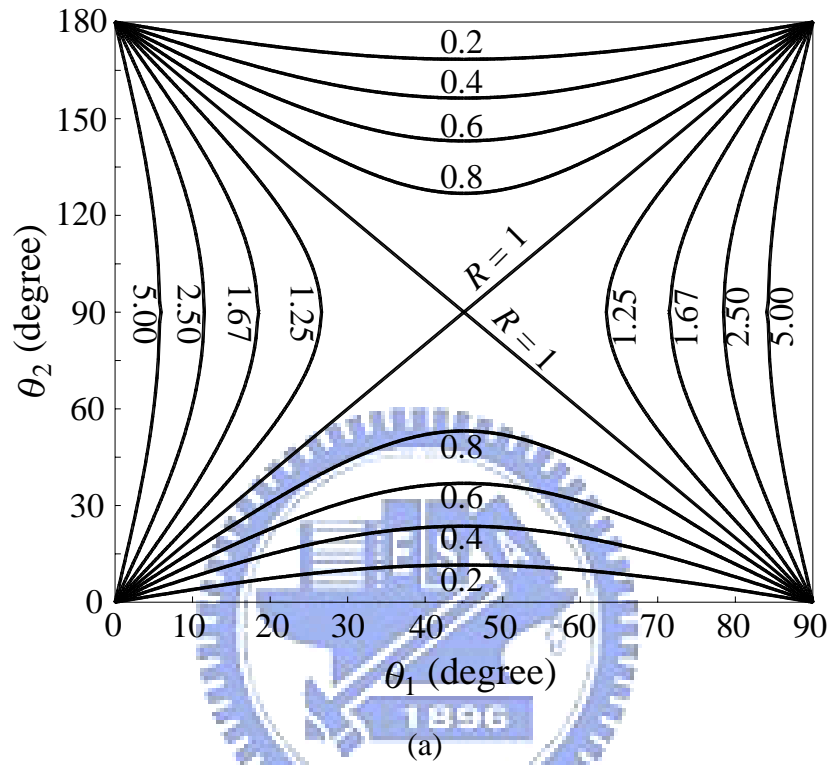
Figure 2.5 (a) θ_2 and (b) Y_1^{-1} solutions as functions of θ_1 for various R values when $|\alpha|$

$= 1$. (c) Normalized total circumference. The θ_1 and θ_2 values are the electric lengths

of the sections evaluated at the operation frequency.

2.2.2 Simulation and measurement

Figure 2.6 compares simulation and measured responses of a rat race coupler, built on a substrate with $\varepsilon_r = 2.2$ and thickness = 0.508 mm, with $\ell = 0.97\lambda$ at $f_o = 2.5$ GHz. The ring has a mean radius of 13.47 mm and a normalized area of $(0.97/1.5)^2 = 41.82\%$. Important circuit parameters include $\theta_1 = 9.4^o$, $\theta_2 = 65.8^o$, $\theta_3 = 99.4^o$, and $R = 2.83$. The simulation is done by the IE3D [18]. The magnitude responses are in Figure 2.6(a), and the relative phases in Figure 2.6(b). At f_o, the measured $|S_{11}|$, $|S_{21}|$, $|S_{31}|$ (isolation) and $|S_{41}|$ are -21.4 dB, -3.37 dB, -29.56 dB and -3.36 dB, respectively. The best measured $|S_{11}|$ is -33.9 dB at 2.47 GHz. The measured results show good agreement with the simulation. Figure 2.6(c) shows the photo of the measured circuit.
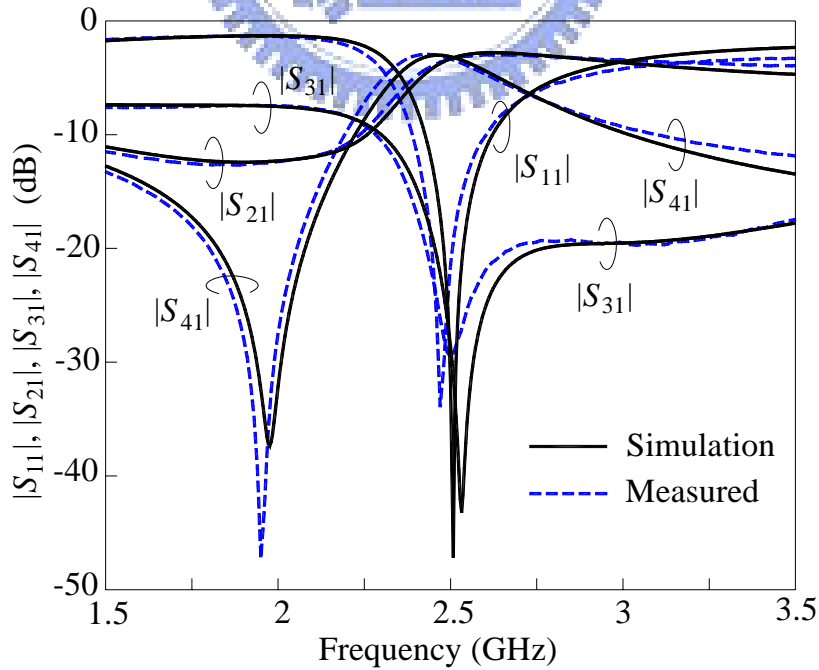
(a)
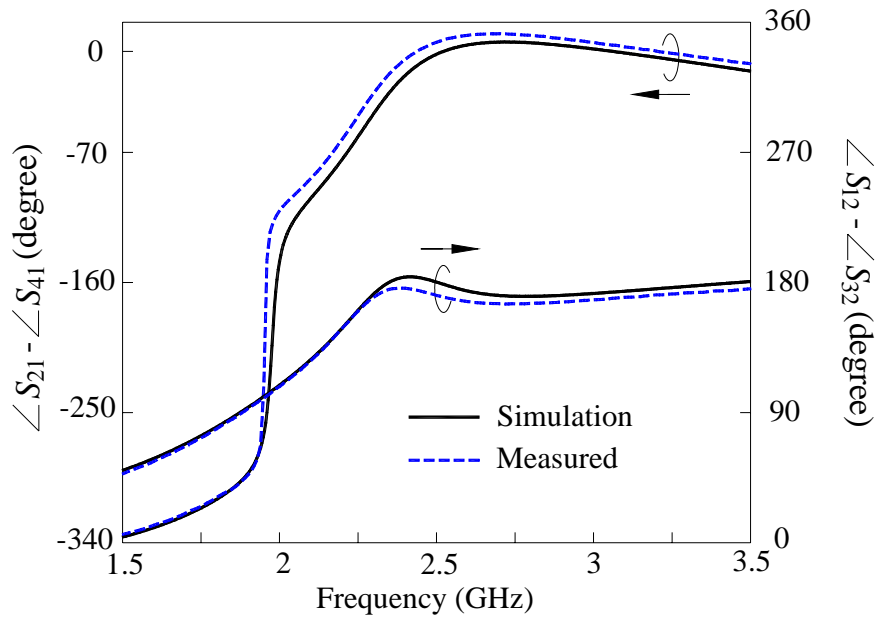
(b)
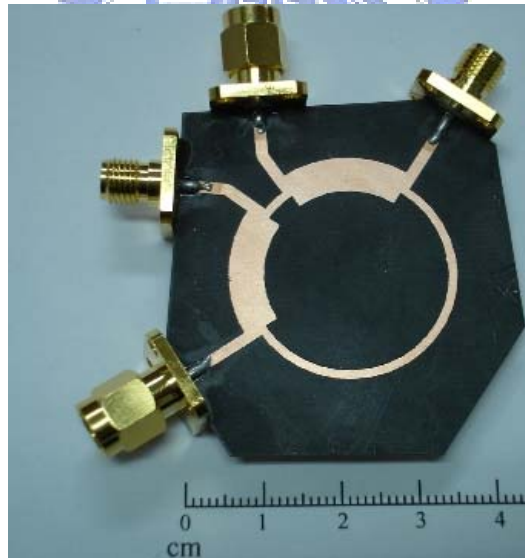
(c)

Figure 2.6 Performances of the experimental rat race coupler. (a) Magnitude responses. (b) Phase responses. (c) Photo of the circuit. $Y_1^{-1} = 62.15\ \Omega$ ($W_1 = 1.09$ mm), $Y_2^{-1} = 21.96\ \Omega$ ($W_2 = 4.64$ mm), $\theta_1 = 9.4^{o}$, $\theta_2 = 65.8^{o}$, $\theta_3 = 99.4^{o}$.

Figure 2.7 plots the simulation bandwidths of the new rat race rings. Although the entire circuit has four stepped-impedance junctions, only the circuits with $R = 5$ and 0.2 need slight trimming for tuning the $|S_{31}|$ dips at $f_o = 2.5$ GHz. A ring with $R = 0.2$ is used for test the circuit bandwidth. The parameters are $\theta_1 = 33.8^o$, $\theta_2 = 10.7^o$, $\theta_3 = 123.8^o$, $Y_1^{-1} = 20.48$ Ω and $Y_2^{-1} = 102.39$ Ω. The bandwidths measured by $|S_{11}| = -15$ dB, $|S_{31}| = -20$ dB, $|S_{12}/S_{32}| = \pm0.5$ dB, $|S_{21}/S_{41}| = \pm0.5$ dB, $\angle S_{21} - \angle S_{41} = \pm5^o$ and $\angle S_{12} - \angle S_{32} = 180^o \pm 5^o$ are 6.8%, 28.9%, 24.8%, 8.8%, 8.8% and 8.5%, respectively. The bandwidth by $|S_{11}| = -15$ dB has the smallest value, so that it is used as a basis in Figure 2.7 for demonstration. When $\theta_1 \le 45^o$, for a given R value, a larger θ_1 has a larger bandwidth, except for $R = 1$ and $\theta_1 \ge 35^o$. For example, when $R = 1.25$, the bandwidth changes from 5% to 35% when θ_1 is varied from 20° to 25°. One can see that when R or $1/R$ is larger, the circuit possesses smaller bandwidth. It is interesting to note that a uniform hybrid ring ($R = 1$) can have a bandwidth from about 5% to 40% by choosing a proper θ_1.
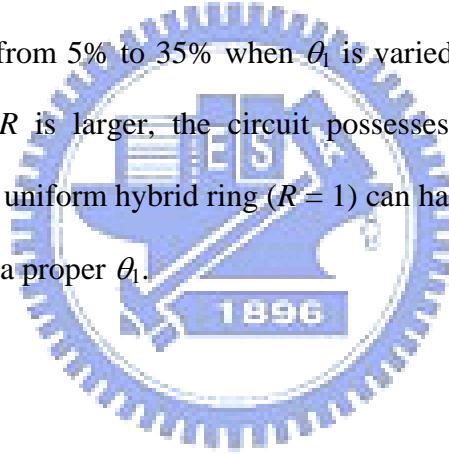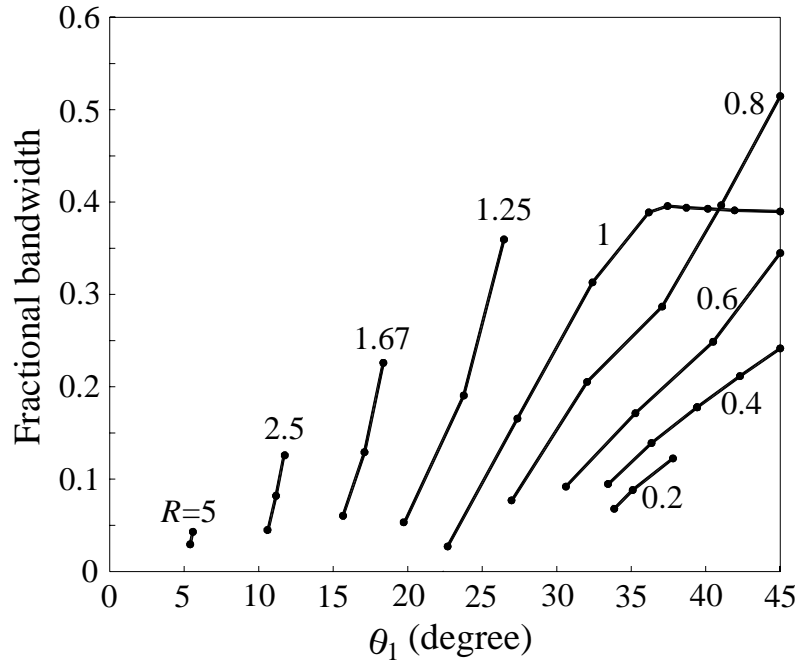
Figure 2.7 Bandwidths of the new rat race couplers. Bandwidth is defined by the frequencies where $|S_{11}| = -15$ dB. Substrate: $\varepsilon_r = 2.2$ and thickness = 0.508 mm.

To show more details on the tradeoffs between bandwidth and normalized circumference ($\underline{\Phi}$ in (2.16)), Table 2.1 summarizes the data shown in Figure 2.5(c) and Figure 2.7. For the extreme cases of $R = 0.2$ and $R = 5$, some line widths are too small to be accepted for simulation so that not all solutions in Figure 2.5(c) are given in Figure 2.7 and Table 2.1. In Table 2.1, $\underline{\Phi}_L$ and $\underline{\Phi}_H$ denote the lower and upper limits of $\underline{\Phi}$ in our simulation, and Δ_L and Δ_H are their bandwidths, respectively. It is noted that $\underline{\Phi}_L$ and $\underline{\Phi}_H$ will change when the substrate or the design frequency is changed.

TABLE 2.1 TRADEOFFS BETWEEN BANDWIDTH AND NORMALIZED CIRCUMFERENCE OF

THE RAT RACE COUPLER

R	$\underline{\Phi}$ (See (2.16))		Δ (%, $|S_{11}| = -15$DB)	
	$\underline{\Phi}_L$	$\underline{\Phi}_H$	Δ_L	Δ_H
0.2	0.62	0.65	6.80	12.2
0.4	0.66	0.75	9.50	24.2
0.6	0.68	0.80	9.20	34.5
0.8	0.68	0.86	7.70	51.5
1.0	0.67	1.00	2.70	39.0
1.25	0.68	0.85	5.40	36.0
1.67	0.67	0.79	6.10	22.6
2.5	0.65	0.73	4.50	12.6
5.0	0.63	0.65	2.90	4.50

CHAPTER 3

Circuit Miniaturization with Stepped-Impedance Sections

Circuit area occupation is always a critical issue in the microwave frequency band, especially at low frequencies. Therefore, many approaches are proposed to save circuit size, as discussed in Chapter 1. This chapter presents an effective way to miniaturize the size of rat race couplers using stepped-impedance sections. Finally, effectiveness of the miniaturization on the circuit bandwidths is also discussed.

3.1 CIRCUIT MINIATURIZATION

3.1.1 Stepped-impedance section

The technique in [13] is employed here to further miniaturize the hybrid ring in Figure 2.6.
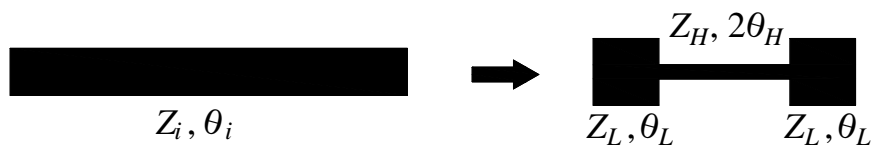

Figure 3.1 Substitution of a uniform section by a stepped-impedance section for circuit miniaturization.

As mentioned in [13], a uniform transmission line is equivalent to a section of

stepped-impedance transmission line as long as they have the same *ABCD* matrix at the designed frequency. Figure 3.1 shows a uniform transmission line section with characteristic impedance Z_i and electric length θ_i, which will be substituted for a stepped-impedance section on the right. The substitution has two sections with characteristic impedance Z_L and electric length θ_L at both ends and a section with characteristic impedance Z_H and electric length $2\theta_H$ in between. The *ABCD* matrix of the stepped-impedance section can be derived as

$$A = D = \cos 2\theta_H \cos 2\theta_L - X \sin 2\theta_H \sin 2\theta_L \tag{3.1a}$$

$$B = jZ_L \left[\cos 2\theta_H \sin 2\theta_L + \sin 2\theta_H \left(X \cos 2\theta_L + K \right) \right] \tag{3.1b}$$

$$C = \frac{j}{Z_L} \left[\cos 2\theta_H \sin 2\theta_L + \sin 2\theta_H \left(X \cos 2\theta_L - K \right) \right] \tag{3.1c}$$

where

$$X = \frac{r + r^{-1}}{2} \tag{3.2a}$$

$$K = \frac{r - r^{-1}}{2} \tag{3.2b}$$

$$r = Z_H / Z_L \tag{3.2c}$$

The next step is to equate (3.1) to the *ABCD* matrix of the uniform transmission line in Figure 3.1 shown in (3.3). Due to circuit symmetry and reciprocity, the conditions $A = D$ and $AD - BC = 1$ can be guaranteed. Therefore, there are only two conditions available in (3.1).

$$A = D = \cos \theta_i \tag{3.3a}$$

$$B = jZ_i \sin \theta_i \tag{3.3b}$$

$$C = \frac{j \sin \theta_i}{Z_i} \tag{3.3c}$$

By equating (3.1a) to (3.3a), we have

$$\cos 2(\theta_H + \theta_L) = \frac{(X-1)\cos 2(\theta_H - \theta_L) + 2\cos \theta_i}{X+1} \tag{3.4}$$

To achieve circuit miniaturization, $\theta_H + \theta_L$ must be as small as possible. Thus, both sides of (3.4) have to be maximized. It results in

$$\theta_H = \theta_L = \frac{1}{4}\cos^{-1}\left(\frac{X-1+2\cos \theta_i}{X+1}\right) \tag{3.5}$$

Let $\theta_0 = \theta_H = \theta_L$, and it can be found that θ_0 is a function of X from (3.5), that is, $(r + r^{-1})/2$. Consequently, both $r = a$ and $r = a^{-1}$ will lead to the same θ_0, where a is an arbitrary real number. $Z_H > Z_L$ ($r > 1$) is chosen herein. Equating (3.1b) to (3.3b), we have

$$Z_L = \frac{2Z_i \sin \theta_i}{(X+1)\sin 4\theta_0 + K \sin 2\theta_0} \tag{3.6}$$

By utilizing (3.5) and (3.6), the four arms of the ring in Figure 2.6 can be replaced by stepped-impedance sections. The $2\theta_1$ arm and each θ_2 arm are substituted for one stepped-impedance section, respectively. However, the $2\theta_3$ arm is replaced by two identical stepped-impedance sections.

Figure 3.2 shows design graphs of the substitutions for Y_1-section (62.15Ω, 18.8°), Y_2-section (21.96Ω, 65.8°), and Y_3-section (62.15Ω, 198.8°) of Figure 2.6(c), respectively. Z_L and Z_H are normalized to Z_0. As shown in Figure 3.2, it can be observed that the larger the value r is, the smaller the section θ_0 is. Therefore, to minimize circuit area, r must be as large as possible. Nevertheless, large r results in large Z_H, the characteristic impedance of the high impedance section. The line width resolution of our PCB (printed circuit board) process is about 0.15 mm which is 150 Ω for a substrate with $\varepsilon_r = 2.2$ and thickness 0.508 mm. Moreover, large r value also leads to small Z_L which may not be practical. Thus, practical r value has an upper limit. The range of r is set to be from 1 to 10 in Figure 3.2. Table 3.1 displays the circuit parameters of the stepped-impedance substitutions. Note that when the substrate dielectric constant or the design frequency is increased, the ring area becomes smaller and hence improves the size reduction factor.

(a)

(b)

(c)
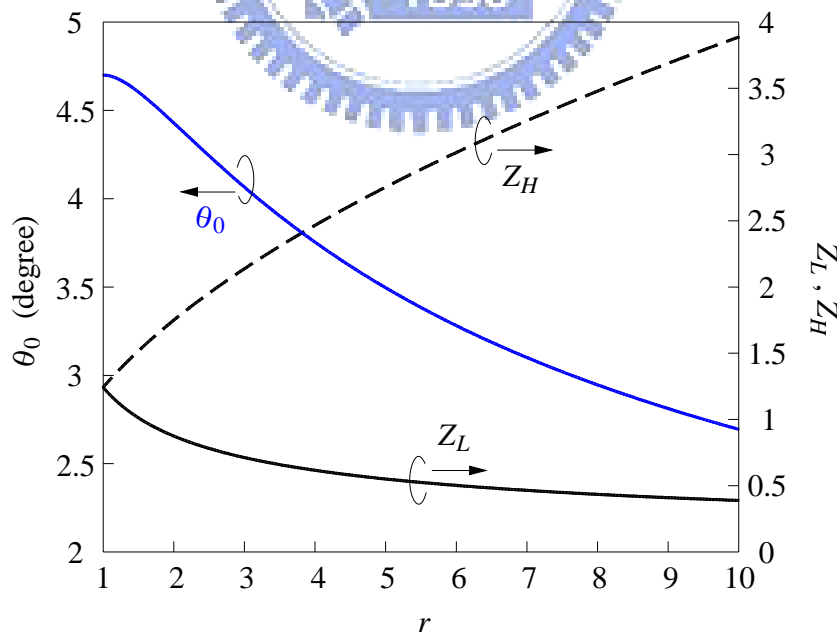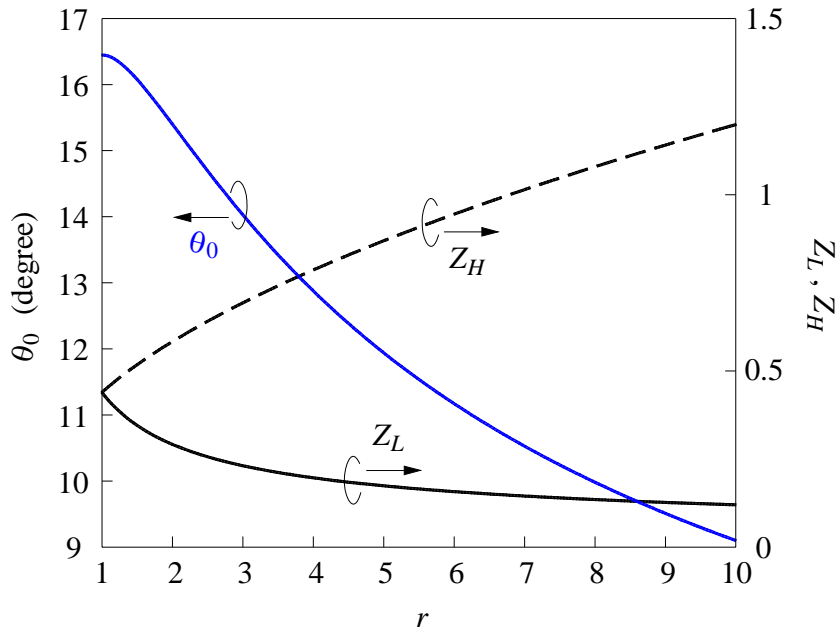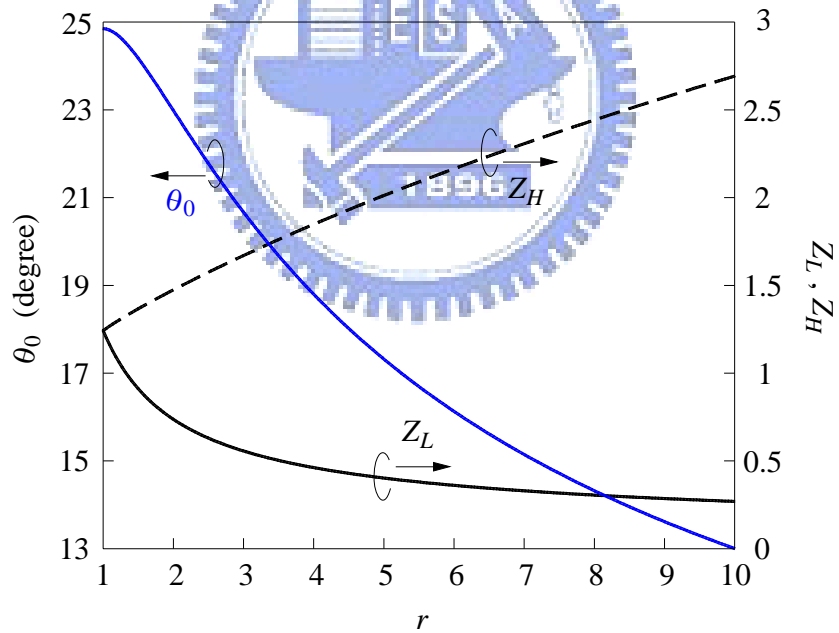
Figure 3.2 θ_0 and normalized impedances Z_L, and Z_H solutions as functions of r in one stepped-impedance section of (a) the Y_1-section, (b) the Y_2-section, and (c) the Y_3-section.

TABLE 3.1 θ_L, Z_L AND Z_H OF THE STEPPED-IMPEDANCE SECTIONS FOR SUBSTITUTING

THE ARMS OF THE RAT RACE COUPLER IN FIGURE 2.6

Section	$\theta_L = \theta_H$	Z_L (Ω)	W_L (mm)	Z_H (Ω)	W_H (mm)
Y_1	3.3^o	25.4	3.89	149.0	0.15
Y_2	9.8^o	6.6	18.03	55.0	1.35
Y_3	13.0^o	13.5	8.24	134.6	0.21

3.1.2 Simulation and measurement

Figure 3.3(a) and 3.3(b) show the performances of a fabricated circuit designed

at 1.03 GHz. The values of θ_L ($=\theta_H$), Z_L and Z_H for the four arms are in Table 3.1. The

length of the Y_1-section of the circuit in Figure 2.6 is $2\theta_1 = 18.8^o$, and the total length

of the stepped-impedance section is only $4\theta_L = 13.2^o$. Similarly, Y_2-section (65.8^o) and

Y_3-section (198.8^o) are replaced by their substitutes of total lengths 39.2^o and 104°,

respectively. Thus the stepped-impedance sections contribute an area reduction factor

of $(195.6^o/349.2^o)^2 = 31.4\%$. The total circumference is 0.54λ and the normalized

circuit area is only 13.12%. The size reduction is much better than that of the

$7\lambda/6$-ring in [13] and believed to be the best miniaturization of planar rat race

couplers in open literature. The measured $|S_{11}|$, $|S_{21}|$, $|S_{31}|$ and $|S_{41}|$ are –22.5 dB, –3.34

dB, –25 dB and –3.56 dB, respectively. The best isolation ($|S_{31}|$) is –35.5 dB at 1.01

GHz. The measured responses are in good agreement with the simulation data. Fig.

3.3(c) shows the photo of the experimental rat race coupler. When the frequency of

the design in Fig. 3.3 is increased to 2.5 GHz, the total stepped-impedance peripheral

becomes 0.78λ and the normalized circuit area is increased to 27.2%, since the ring

area limits the line width of the low-impedance sections.

(a)

(b)
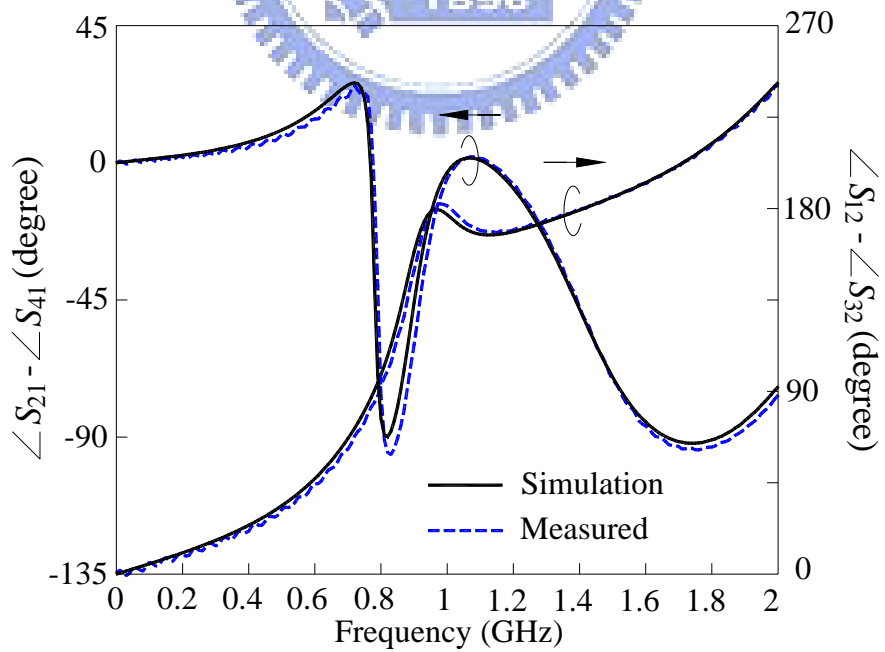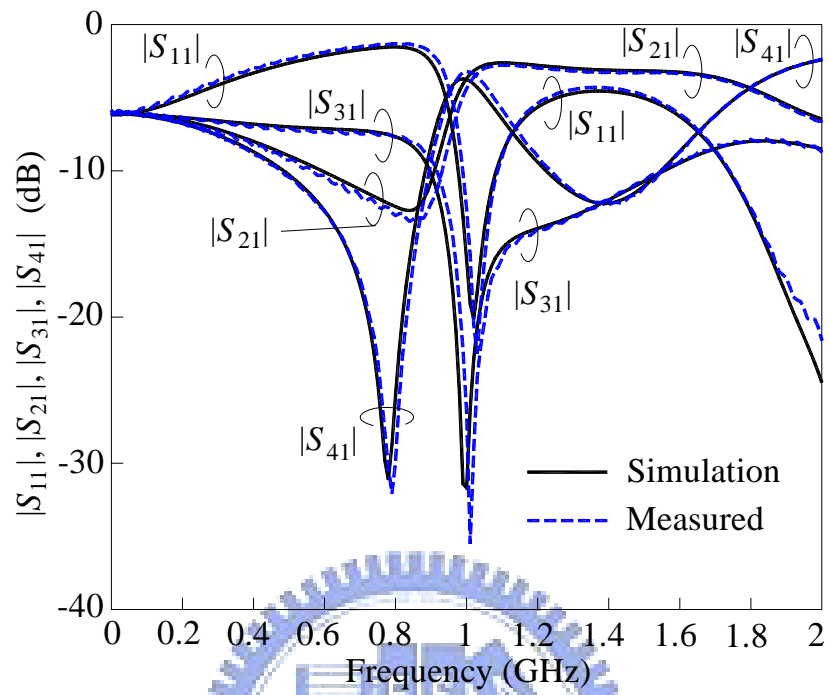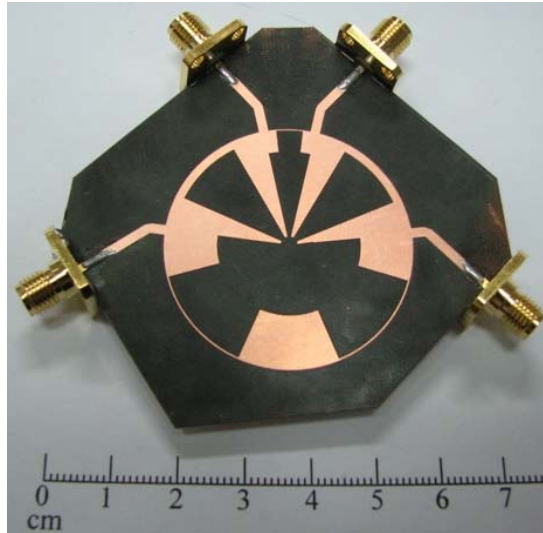
(c)

Figure 3.3 Performances of the 0.54λ-ring coupler. (a) Magnitude responses. (b) Relative phase responses. (c) Photo of the experimental rat race coupler. Geometric parameters are in Table 3.1.
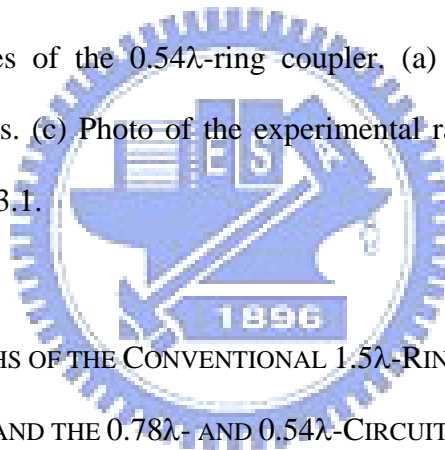
TABLE 3.2   BANDWIDTHS OF THE CONVENTIONAL 1.5λ-RING, THE 0.97λ-RAT RACE IN FIGURE 2.6, AND THE 0.78λ- AND 0.54λ-CIRCUITS IN FIGURE 3.3

Circuit (2.5 GHz)	$|S_{11}| = -15$ dB (Input matching)		$|S_{31}| = -20$ dB (Isolation)		$\angle S_{41} - \angle S_{21} =$ $\pm 5^{o}$		$\angle S_{12} - \angle S_{32} =$ $180^{o} \pm 5^{o}$	
	Sim.	Mea.	Sim.	Mea.	Sim.	Mea.	Sim.	Mea.
1.5λ-ring	39.5%	-	31.3%	-	16.1%	-	15.3%	-
0.97λ-ring	3.9%	4.0%	11.9%	9.4%	5.7%	2.9%	10.8%	2.9%
0.78λ-ring	3.2%	-	5.2%	-	12.4%	-	4.4%	-
0.54λ-ring (1 GHz)	4.6%	3.9%	6.3%	5.9%	16.7%	15.5%	7.2%	9.1%

Table 3.2 compares the bandwidths of the conventional 1.5λ ring, the 0.97λ rat race in Figure 2.6, and the 0.54λ and 0.78λ circuits in Figure 3.3. The leading three circuits are designed at 2.5 GHz. The circuit in Figure 2.6 offers smaller bandwidths than the traditional rat race coupler. In particular, the bandwidths measured by $|S_{11}|$ = –15 dB and $|S_{31}|$ = –20 dB of the circuit in Figure 2.6 are about respectively one tenth and one third of those of the 1.5-λ ring. The simulation bandwidths measured by $\angle S_{41} - \angle S_{21} = \pm 5^{\text{o}}$ and $\angle S_{12} - \angle S_{32} = 180^{\text{o}} \pm 5^{\text{o}}$ of the 0.78λ circuit and that in Figure 2.6 are between 4.4% and 12.4%. A comparison of the data of 0.54λ and 0.78λ in Figure 3.3 shows that ring miniaturized by the stepped-impedance approach at a lower frequency has larger simulation bandwidths.
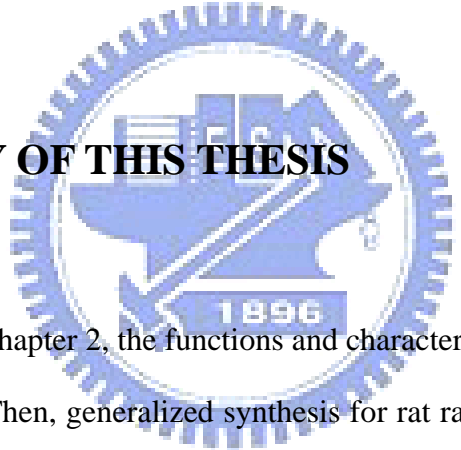
CHAPTER 4

Conclusion

In this thesis, generalized synthesis for a rat race ring coupler is derived and demonstrated. Tradeoffs between peripheral and bandwidth are also clarified. Moreover, to reduce the circuit size, stepped-impedance sections are adopted to replace the arms of a rat race. Bandwidths of the rat race couplers mentioned in this paper are compared. Finally, some suggestions for the advanced research are provided.

4.1 SUMMARY OF THIS THESIS

In the first part of chapter 2, the functions and characteristics of a rat race coupler are briefly introduced. Then, generalized synthesis for rat race couplers is performed. Design equations are provided for calculating the electric lengths and the characteristic impedances of the four arms. There are two degrees of freedom in choosing the geometric parameters for synthesis of the rat race couplers. The upper and lower bounds of the solutions are given in analytical expressions. A 0.97λ-ring operating at 2.5 GHz is then fabricated and measured. Finally, operation bandwidths of the synthesized rat race couplers are simulated and discussed. In general, bandwidth decreases when circumference is reduced. Moreover, larger impedance ratio of the arms leads to better size reduction but a smaller bandwidth.

The arms of a rat race are substituted for stepped-impedance sections to achieve

circuit miniaturization in Chapter 3. By utilizing the technique, the size of 0.97λ-ring is further reduced at 1 GHz. The realized circuit occupies only 13.12% of the area of a conventional 1.5λ-ring and its performances are compared with the 0.97λ-ring and the conventional rat race. In general, the size reduction leads to a decreased circuit bandwidth.

4.2   SUGGESTIONS FOR FUTURE STUDIES

Generalized synthesis of a rat race coupler and its application to circuit miniaturization are presented in this thesis. At least three related topics can be developed for further research. First, as mentioned in Chapter 2, the power ratio of two output ports can be controlled by the impedance ratio (R) and electric lengths (θ_1 and θ_2). Nevertheless, the range of the power ratio is restricted to circuit parameters. If a wide range of $|\alpha|$ ($|S_{21}/S_{41}|$, $|S_{12}/S_{32}|$) is required, the impedance ratio or electric length may be impractical. Additional elements such as shunt stubs can probably solve the problem.

Second, stepped-impedance sections can be utilized for other applications such as rat race couplers with dual-band function. Since stepped-impedance sections provide more degrees of freedom in circuit design, the required conditions for two operation frequencies may be satisfied.

Third, designing a wide bandwidth rat race coupler is also an interesting topic. In general, the fractional bandwidth of a rat race coupler realized in microstrip substrate is less than 60%. It's a challenge to synthesize a microstrip rat race with a bandwidth

more than 60%. Cascading similar elements together generally produces a wider bandwidth than a single element. Consequently, cascading two or more rat race rings can be a possible approach for wide-band application.

References

[1] R. K. Settaluri, G. Sundberg, A. Weisshaar and V. K. Tripathi, "Compact folded line rat-race hybrid couplers," *IEEE Microw. Guided Wave Lett.*, vol. 10, no. 2, pp. 61–63, Feb. 2000.

[2] H.-R. Ahn, I.-S. Chang, and S.-W. Yun, "Miniaturized 3-dB ring hybrid terminated by arbitrary impedances," *IEEE Trans. Microw. Theory Tech.*, vol. 42, pp. 2216–2221, Dec. 1994.

[3] T. Hirota, A. Minakawa, and M. Muraguchi, "Reduced-size branch-line and rat-race hybrids for uniplanar MMICs," *IEEE Trans. Microw. Theory Tech.*, vol. 38, no. 3, pp. 270–275, Mar. 1990.

[4] K. M. Shum, Q. Xue and C. H. Chan, "A novel microstrip ring hybrid incorporating a PBG cell," *IEEE Microw. Wireless Compon. Lett.*, vol. 11, no. 6, pp. 258–260, Jun. 2001.

[5] J. Gu and X. Sun, "Miniaturization and harmonic suppression rat-race coupler using C-SCMRC resonators with distributive equivalent circuit," *IEEE Microw. Wireless Comp. Lett.*, vol. 15, no. 12, pp. 880–882, Dec. 2005.

[6] C. H. Ho, L. Fan and K. Chang, "Broad-band uniplanar hybrid-ring and branch-line couplers," *IEEE Trans. Microw. Theory Tech.*, vol. 41, no. 12, pp. 2116–2125, Dec. 1993.

[7] T. Wang and K. Wu, "Size-reduction and band-broadening design technique of uniplanar hybrid ring coupler using phase inverter for M(H)MIC's," *IEEE Trans. Microw. Theory Tech.*, vol. 47, no. 2, pp. 198–206, Feb. 1999.

[8] C.-W. Kao and C.-H. Chen, "Novel uniplanar 180° hybrid-ring couplers with spiral-type phase inverters," *IEEE Microw. Guided Wave Lett.*, vol. 10, no. 10, pp. 412–414, Oct. 2000.

[9] Y. J. Sung, C. S. Ahn and Y.-S. Kim, "Size reduction and harmonic suppression of rat-race hybrid coupler using defected ground structure," *IEEE Microw. Wireless Comp. Lett.*, vol. 14, no. 1, pp. 7–9, Jan. 2004.

[10] M.-L. Chuang, "Miniaturized ring coupler of arbitrary reduced size," *IEEE Microw. Wireless Comp. Lett.*, vol. 15, no. 1, pp. 16–18, Jan. 2005.

[11] K. W. Eccleston and S. H. M. Ong, "Compact planar microstripline branch-line and rat-race coupler," *IEEE Trans. Microw. Theory Tech.*, vol. 51, pp. 2119–2125, Oct. 2003.

[12] D. I. Kim and G. S. Yang, "Design of new hybrid-ring directional coupler using λ/8 or λ/6 sections," *IEEE Trans. Microw. Theory Tech.*, vol. 39, no. 10, pp. 1779–1783, Oct. 1991.

[13] J.-T. Kuo, J.-S. Wu and Y.-C. Chiou, "Miniaturized rat race coupler with suppression of spurious passband," *IEEE Microw. Wireless Compon. Lett.*, vol. 17, no. 1, pp. 46–48, Jan. 2007.

[14] C.-L. Hsu, C.-W. Chang and J.-T. Kuo, "Design of dual-band microstrip rat race coupler with circuit miniaturization," *IEEE MTT-S Int. Microwave Symp.*, Honolulu, Hawaii, USA, June 3-8, 2007, pp. 177–180.

[15] C.-L. Hsu, J.-T. Kuo and C.-W. Chang, "Miniaturized dual-band hybrid couplers with arbitrary power division ratios," *IEEE Trans. Microw. Theory Tech.*, vol. 57, no. 1, pp. 149–156, Jan. 2009.

[16] M. K. Mandal and S. Sanyal, "Reduced-length rat-race couplers," *IEEE Trans. Microw. Theory Tech.*, vol. 55, no. 12, pp. 2593–2598, Dec. 2007.

[17] M.-H. Murgulescu, E. Penard, I. Zaquine, "Design formulas for generalised 180$^{\text{o}}$ hybrid ring couplers," *Electron. Lett.*, vol. 30, no.7, pp. 573–574, Mar. 1994.

[18] *IE3D Simulator*, Zeland Software Inc., Jan. 1997.

[19] D. M. Pozar, *Microwave Engineering*, 2nd ed. New York: Wiley, 1998.